Journal of Engineering Science and Technology
Vol. 12, No. 2 (2017) 471 - 490

FINITE ELEMENT APPROACH AND MATHEMATICAL FORMULATION OF VISCOELASTIC AUXETIC HONEYCOMB STRUCTURES FOR IMPACT MITIGATION

MOZAFAR SHOKRI RAD[1], SAEID MOHSENIZADEH[2], ZAINI AHMAD[2,*]

[1]Faculty of Engineering, Lorestan University, Khorramabad, Iran
[2]Department of Applied Mechanics & Design, Faculty of Mechanical Engineering, Universiti Teknologi Malaysia, 81310 Johor Bahru, Malaysia
*Corresponding Author: azaini@mail.fkm.utm.my

Abstract

Auxetic structures are designed to be used for producing auxetic materials with controllable mechanical properties. The present study treats a design of viscoelastic auxetic honeycomb structures using numerical approach and mathematical formulation for impact mitigation. In order to increase the energy absorption capacity, viscoelastic material has been added into auxetic structure as it has capability to dissipate energy under impact loading. Kelvin-Voigt and Maxwell models were employed to model viscoelastic components. The auxetic structure was then subjected to impact load with linear and nonlinear load functions. Dynamic analysis was carried out on a star honeycomb structure using continuum mechanics. Influence of different parameters on response function was then further studied. The primary outcome of this research is the development of viscoelastic auxetic honeycomb structural design for predicting the impact resistance under impact loading.

Keywords: Viscoelastic, Analytical, Auxetic structure, Energy absorption, Dynamic loading.

1. Introduction

As opposed to purely elastic materials, a viscoelastic material has both elastic and viscous components. Pure elastic materials do not lose energy (heat) under dynamic loadings [1, 2]. However, a viscoelastic material loses energy when loaded and unloaded.

There are two types of viscoelastic materials: linear and nonlinear. Linear viscoelasticity is used for separable function while nonlinear is used when the

Nomenclatures

a_{G1}	Acceleration of point G_1
C	Damping of viscoelastic material
$f_1(t)$	Impact loading function, N
$f_2(t)$	Damping coefficient of viscoelastic component
F_c	Damper force, N
Fs	Spring force, N
h	Initial value of Y_q with respect to XY coordinate system
H	Initial value of Y_n with respect to XY coordinate system
K	Stiffness of viscoelastic material
K'	Stiffness coefficient of sparing designed for setting θ at θ_0
L_1	Length of parts $\overline{AB}, \overline{AF}, \overline{CD}$ and $\overline{DE}$, m
m_1	Mass of parts $\overline{AB}, \overline{AF}, \overline{CD}$ and $\overline{DE}$, Kg
(X_A,Y_A)	Coordinate of point A with respect to XY coordinate system
(X_n,Y_n)	Coordinate of point n with respect to XY coordinate system

Greek Symbols

θ	Angle of part $\overline{AB}$ with respect to horizontal direction, deg
θ_0	Initial value of θ deg

function is not separable. Nonlinear often happens when the deformations are large or when mechanical properties of the material change during deformation. These materials need to be modelled to obtain their stress or strain interactions. These models including the Kelvin-Voigt model, Maxwell model and the Standard Linear Solid Model are used to predict a material's response under different loading conditions. The Kelvin–Voigt model consists of a Newtonian damper and Hookean elastic spring connected in parallel. The Maxwell model can be represented by a purely viscous damper and a purely elastic spring connected in series. The Standard Linear Solid Model effectively combines the Maxwell Model and a Hookean spring in parallel. A viscous material is modelled as a spring and a dashpot in series with each other, both of which are in parallel with a lone spring.

Moreover, auxetic materials are new class of materials exhibiting negative Poisson's ratio. Using characteristics of these materials, they are beneficial for many applications. Studies and experiments have proven that these materials have the ability to improve important mechanical properties such as shear modulus, fatigue crack propagation, energy absorption, impact resistance, fracture toughness, and indentation resistance [3, 4]. There are two types of auxetic materials which are man-made auxetic and natural auxetic [5, 6].

For decades, several geometrical structures with the auxetic behaviour have been introduced, fabricated and tested for their mechanical properties. These geometrical structures are considerably indispensable as they could be used to comprehend how auxeticity effects could be achieved and how auxetic materials can be manufactured as well as how their properties can be optimized and predicted [7]. Most importantly, they can be used to produce auxetic materials with controllable mechanical properties.

Among the most important classes of auxetic structures are re-entrant structures [5-7], chiral structures [8, 9], rotating rigid/semi-rigid units [10-12], angle-ply laminates [13, 14], hard molecules [15-17], micro porous polymers [18-20] and liquid crystalline polymer [21-23]. Re-entrant structures have attracted more attention compared to other structures owing to their ability to model auxetic materials. Star honeycomb structure is one of the important re-entrant structures of auxetic materials [5] and such structure has been tailored in the present study. This structure is made of 12 beams with the same length and same cross section as shown in Fig. 1(a).

The most important applications of this structure are to be used as cellular structure of an auxetic material with controllable mechanical properties both in 2D and 3D cases as shown in Fig. 1(b). Energy absorbing potential of viscoelastic materials makes them an excellent choice in the man-made auxetic industry [24-25]. The viscoelastic material is added to the auxetic structure in order to re-increase the energy absorption capability. Therefore, using viscoelastic materials in man-made auxetic industry seems to be a necessity.

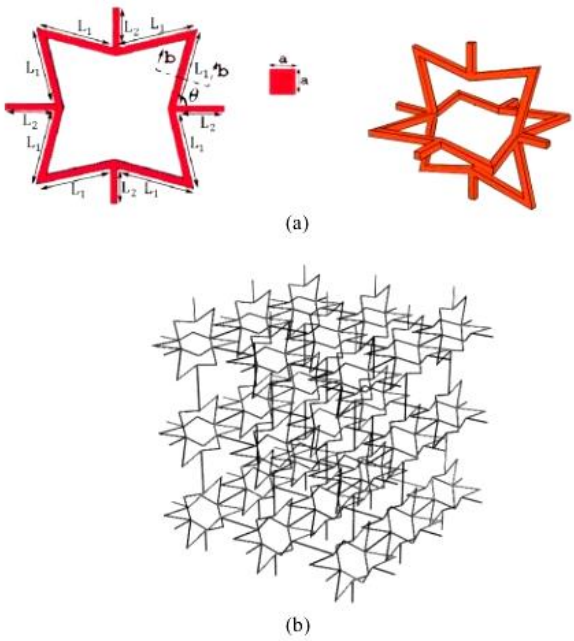

Fig. 1. (a) Star-shaped structure in 2D and 3D.
(b) An element of auxetic material made of 3D star-shaped structures.

In this present study, a design of viscoelastic auxetic honeycomb structures for impact mitigation has been established. In order to increase the energy absorption capacity of the auxetic structure, viscoelastic material has been adopted to form auxetic structure as it has the ability to dissipate energy under dynamic loading. A collection of star honeycomb structures was taken into consideration to act as an auxetic structure. Kelvin-Voigt and Maxwell models were employed to model viscoelastic component. The auxetic structure was then subjected to impact load with linear and nonlinear load functions. Dynamic analysis was carried out on a star honeycomb structure using continuum mechanics. Numerical analysis was

carried out to solve nonlinear coupled differential equations obtained from dynamic analysis. Influence of different parameters on response function was then further studied. The primary outcome of this research is the development of empirical formulation for calculating the impact resistance of viscoelastic auxetic structure under dynamic loading.

2. Development of Auxetic Model

2.1. Definition of the model

The model is defined as star honeycomb structures in which viscoelastic component has been used. To make the structure easier to be analysed, it was considered as six rigid parts connected each other by hinge joints as shown in Fig. 2. In Fig. 2, $\overline{AB}$, $\overline{AF}$, $\overline{CD}$ and $\overline{DE}$ are straight rigid parts with the same length of L_1, and the same mass of m_1. Also, parts $\overline{BC}$ and $\overline{EF}$ are rigid parts made of three straight parts. Effect of elasticity and viscosity of the material was also considered as a linear spring and damper inside the structure. To analyse the structure dynamically, Kelvin–Voigt and Maxwell models were used for modelling material's viscoelasticity (see Fig. 2). The viscoelastic components were situated inside the structure, resulting in reducing the impact load, they translate the load to another structure using a slender rigid rod passing through part $\overline{EF}$ as shown in Fig. 2.

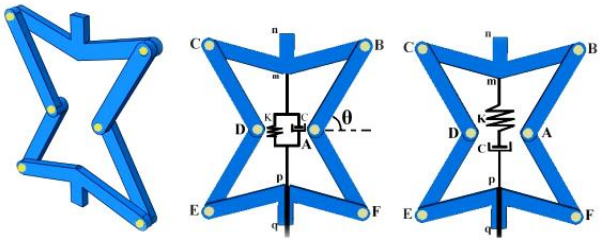

Fig. 2. Viscoelastic models of auxetic structure using rigid parts and linear spring and damper.

Although attempt has been done to reduce the degrees of freedom by reducing the number of hinge joints, the number of freedom's degrees is still three [26]. A collection of the defined structure was considered as an auxetic material with controllable ability of energy absorption (see Fig. 3). In Fig. 3, the horizontal springs were weak enough to be neglected in calculations. The aim of designing them is setting initial θ at a desired value. However, since any structure has three degrees of freedom, the number of degrees of freedom for such a model is great. This makes the calculation too much complicated due to the nonlinearity of dynamic equations. Therefore, in here, one structure for dynamic analysis was considered in which the slender rigid rod was fixed to a foundation as shown in Fig. 4. Fixing the rod causes reduction of the degrees of freedom to two. As seen in this figure, impact loading, $f_1(t)$ was applied to the structure. Then, dynamic

analysis was carried out to obtain the function of transmitted load to the foundation, $f_2(t)$.

Neglecting the weights of all parts of the structure, body force diagrams of them is shown in Fig. 5. In this figure, in the case of Kelvin-Voigt model: $F = F_S + F_C$, and in the case of Maxwell model: $F = F_S = F_C$, where F_S and F_C are spring and damper forces, respectively.

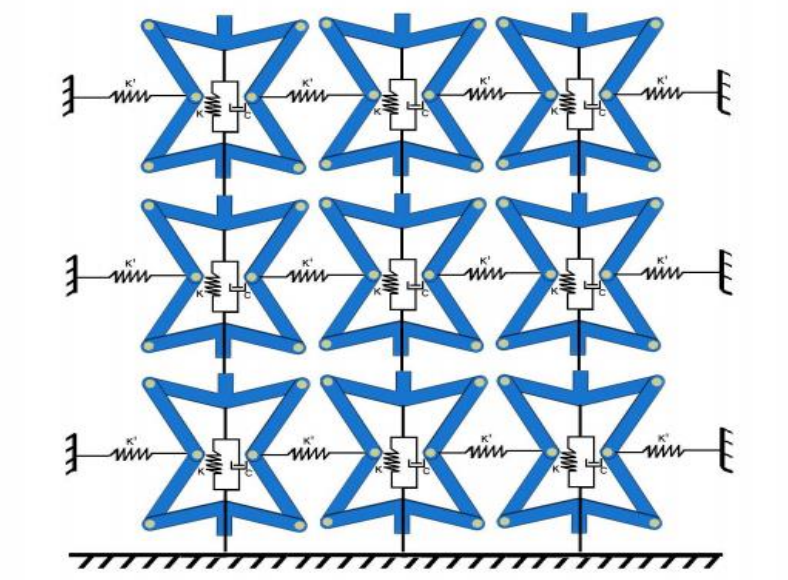

Fig. 3. A collection of the defined structure for modeling behavior of viscoelastic auxetic material when impacted.

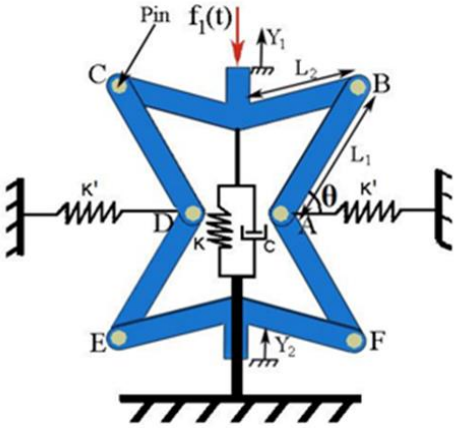

Fig. 4. A structure used for modelling auxetic material.

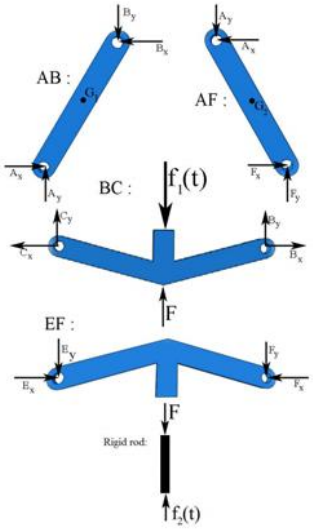

Fig. 5. Body force diagram of all parts of the structure.

2.2. Dynamic analysis of the model

In Fig. 6, the following equation is written among different points located on the structure in *x-y* coordinate system:

$$Y_n - Y_q = Y_{n/q} = Y_{n/m} + Y_{m/B} + Y_{B/A} + Y_{A/F} + Y_{F/p} + Y_{p/q} \tag{1}$$

where $Y_n = Y_1 + H$, $Y_q = Y_2 + h$, $H - h = 2L_1 \sin\theta_0$, $Y_{n/m} = c_1$, $Y_{m/B} = -c_1$, $Y_{B/A} = Y_{A/F} = L_1 \sin\theta$, $Y_{F/p} = -c_1$ and $Y_{p/q} = c_1$

After substitution and simplification, the relationship among Y_1 , Y_2 and θ is written as:

$$Y_1 = Y_2 + 2L_1\left(\sin\theta - \sin\theta_0\right) \tag{2}$$

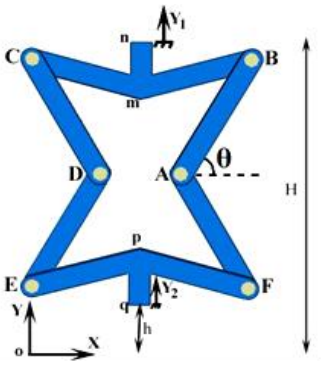

Fig. 6. Coordinate *XY* system, Y_1 , and Y_2 defined for dynamic analysis of the structure.

The above equation decreases the degrees of freedom from three (3) to two (2). In Fig. 6, coordinates of joint A in *x*-*y* coordinate system is also written as:

$$\left.\begin{aligned} &X_A = X_{A/O} = X_{A/F} + X_{F/p} + X_{p/q} + X_{q/O} \\ &\Rightarrow X_A = -L_1\cos\theta_1 + c_1 + 0 + 0 = -L_1\cos\theta \\ &Y_A = Y_{A/O} = Y_{A/F} + Y_{F/p} + Y_{p/q} + Y_{q/O} \\ &\Rightarrow Y_A = L_1\sin\theta + Y_2 + c \end{aligned}\right\} \quad (3)$$

Two times derivation of displacements X_A and Y_A with respect to y yields the acceleration of A along *x* and *y* directions as follows:

$$\left.\begin{aligned} &(a_A)_x = \ddot{X}_A = L_1\left[\ddot{\theta}\sin\theta + \dot{\theta}^2\cos\theta\right] \\ &(a_A)_Y = \ddot{Y}_A = L_1\left[\ddot{\theta}\cos\theta - \dot{\theta}^2\sin\theta\right] + \ddot{Y}_2 \end{aligned}\right\} \quad (4)$$

Taking into consideration the $F = F_S = F_C$ rigidity of part $\overline{AB}$, the following equation can be written:

$$\begin{aligned} &\vec{a}_{G_1} = \vec{a}_A + \left(\dot{\theta}\vec{k}\right)\times\left[\left(\dot{\theta}\vec{k}\right)\times\left[\left(\frac{L_1}{2}\cos\theta\right)\vec{i} + \left(\frac{L_1}{2}\sin\theta\right)\vec{j}\right]\right] \\ &+\left(\ddot{\theta}\vec{k}\right)\times\left[\left(\frac{L_1}{2}\cos\theta\right)\vec{i} + \left(\frac{L_1}{2}\sin\theta\right)\vec{j}\right] \end{aligned} \quad (5)$$

where $\vec{a}_{G_1}$ and $\vec{a}_A$ are accelerations of points G_1 and A, respectively. This equation gives the components of $\vec{a}_{G_1}$ along *x* and *y* directions as follows:

$$\left.\begin{aligned} &\left(a_{G_1}\right)_X = \frac{L_1}{2}\left[\ddot{\theta}\sin\theta + \dot{\theta}^2\cos\theta\right] \\ &\left(a_{G_1}\right)_Y = \frac{3L_1}{2}\left[\ddot{\theta}\sin\theta - \dot{\theta}^2\cos\theta\right] + \ddot{Y}_2 \end{aligned}\right\} \quad (6)$$

Similarly, the following equation can be written for part $\overline{AF}$ as follows:

$$\begin{aligned} &\vec{a}_{G_2} = \vec{a}_A + \left(-\dot{\theta}\vec{k}\right)\times\left[\left(-\dot{\theta}\vec{k}\right)\times\left[\left(\frac{L_1}{2}\cos\theta\right)\vec{i} - \left(\frac{L_1}{2}\sin\theta\right)\vec{j}\right]\right] \\ &+\left(-\ddot{\theta}\vec{k}\right)\times\left[\left(\frac{L_1}{2}\cos\theta\right)\vec{i} - \left(\frac{L_1}{2}\sin\theta\right)\vec{j}\right] \end{aligned} \quad (7)$$

The above equation gives the components $\vec{a}_{G_2}$ along *x* and *y* directions as follows:

$$\left.\begin{aligned} &\left(a_{G_2}\right)_X = \frac{L_1}{2}\left[\ddot{\theta}\sin\theta + \dot{\theta}^2\cos\theta\right] \\ &\left(a_{G_2}\right)_Y = \frac{L_1}{2}\left[\ddot{\theta}\cos\theta - \dot{\theta}^2\sin\theta\right] + \ddot{Y}_2 \end{aligned}\right\} \quad (8)$$

Also, the same equation is written for points A and B in part $\overline{AB}$:

$$\left.\begin{aligned}
&\vec{a}_B = \vec{a}_A + \left(\dot{\theta}\vec{k}\right)\times\left[\left(\dot{\theta}\vec{k}\right)\times\left[\left(L_1\cos\theta\right)\vec{i} + \left(L_1\sin\theta\right)\vec{j}\right]\right] \\
&+\left(\ddot{\theta}\vec{k}\right)\times\left[\left(L_1\cos\theta\right)\vec{i} + \left(L_1\sin\theta\right)\vec{j}\right] \\
&\vec{a}_F = \vec{a}_A + \left(-\dot{\theta}\vec{k}\right)\times\left[\left(-\dot{\theta}\vec{k}\right)\times\left[\left(\frac{L_1}{2}\cos\theta\right)\vec{i} - \left(\frac{L_1}{2}\sin\theta\right)\vec{j}\right]\right] \\
&+\left(-\ddot{\theta}\vec{k}\right)\times\left[\left(\frac{L_1}{2}\cos\theta\right)\vec{i} - \left(\frac{L_1}{2}\sin\theta\right)\vec{j}\right]
\end{aligned}\right\} \quad (9)$$

Because of the symmetry of the structure, parts $\overline{AB}$ and $\overline{EF}$ move along Y direction. Therefore, using Eq. (9), acceleration of B and F can be written as:

$$\left.\begin{aligned}
&a_B = \left(a_B\right)_Y = 2L_1\left[\ddot{\theta}\cos\theta - \dot{\theta}^2\sin\theta\right] + \ddot{Y}_2 \\
&a_F = \left(a_F\right)_Y = \frac{L_1}{2}\left[\ddot{\theta}\cos\theta\right] + \ddot{Y}_2
\end{aligned}\right\} \quad (10)$$

After determining the accelerations, force analysis of parts is dealt with. First, using body force diagram of part $\overline{AB}$ and obtained acceleration of G_1, dynamic equations of this part are written as:

$$\left.\begin{aligned}
&\Sigma F_X = m_1\left(a_{G_1}\right)_X \Rightarrow A_X - B_X \\
&= \frac{m_1L_1}{2}\left[\ddot{\theta}\sin\theta + \dot{\theta}^2\cos\theta\right] \\
&\Sigma F_Y = m_1\left(a_{G_1}\right)_Y \Rightarrow A_Y - B_Y \\
&= \frac{3m_1L_1}{2}\left[\ddot{\theta}\cos\theta - \dot{\theta}^2\sin\theta\right] + m_1\ddot{Y}_2 \\
&\Sigma M_{G_1} = I_{G_1}\ddot{\theta} \Rightarrow \left(\frac{L_1}{2}\sin\theta\right)\left[A_X + B_X\right] \\
&-\left(\frac{L_1}{2}\cos\theta\right)\left[A_Y + B_Y\right] = \frac{m_1L_1^2}{12}\ddot{\theta}
\end{aligned}\right\} \quad (11)$$

Then, dynamic force equations of part $\overline{EF}$ are similarly written as:

$$\left.\begin{aligned}
&\Sigma F_X = m_1\left(a_{G_2}\right)_X \Rightarrow F_X - A_X \\
&= \frac{m_1L_1}{2}\left[\ddot{\theta}\sin\theta + \dot{\theta}^2\cos\theta\right] \\
&\Sigma F_Y = m_1\left(a_{G_2}\right)_Y \Rightarrow F_Y - A_Y \\
&= \frac{m_1L_1}{2}\left[\ddot{\theta}\cos\theta - \dot{\theta}^2\sin\theta\right] + m_1\ddot{Y}_2 \\
&\Sigma M_{G_2} = I_{G_2}\left(-\ddot{\theta}\right) \Rightarrow \left(\frac{L_1}{2}\sin\theta\right)\left[A_X + F_X\right] \\
&+\left(\frac{L_1}{2}\cos\theta\right)\left[A_Y + F_Y\right] = -\frac{m_1L_1^2}{12}\ddot{\theta}
\end{aligned}\right\} \quad (12)$$

Now, the system in Eqs. (11) and (12) are written in matrix forms as follows:

$$\begin{bmatrix} 1 & 0 & -1 & 0 & 0 & 0 \\ \left(\frac{L_1}{2}\sin\theta\right) & \left(\frac{L_1}{2}\sin\theta\right) & \left(\frac{L_1}{2}\sin\theta\right) & \left(\frac{L_1}{2}\sin\theta\right) & 0 & 0 \\ -1 & 0 & 0 & 0 & 1 & 0 \\ 0 & -1 & 0 & 0 & 0 & 1 \\ \left(L_1\sin\theta\right) & \left(L_1\cos\theta\right) & 0 & 0 & 0 & 0 \end{bmatrix} \begin{bmatrix} A_X \\ A_Y \\ B_X \\ B_Y \\ F_X \\ F_Y \end{bmatrix} =$$

$$\begin{bmatrix} \frac{m_1L_1}{2}\left(\ddot{\theta}\sin\theta+\dot{\theta}^2\cos\theta\right) \\ \frac{3m_1L_1}{2}\left(\ddot{\theta}\cos\theta-\dot{\theta}^2\sin\theta\right)+m_1\ddot{Y}_2 \\ \left(\frac{m_1L_1^{\,2}}{12}\right)\ddot{\theta} \\ \frac{m_1L_1}{2}\left(\ddot{\theta}\sin\theta+\dot{\theta}^2\cos\theta\right) \\ \frac{m_1L_1}{2}\left(\ddot{\theta}\cos\theta-\dot{\theta}^2\sin\theta\right)+m_1\ddot{Y}_2 \\ \left(-\frac{m_1L_1^{\,2}}{12}\right)\ddot{\theta} \end{bmatrix} \tag{13}$$

2.3. Dynamic force equations for Kelvin–Voigt model

In this model, dynamic force equations of part $\overline{BC}$ are written as:

$$\begin{aligned} &\sum F_X = 0 \Rightarrow C_X = B_X \\ &\sum F_Y = m_2 a_B \Rightarrow -f_1(t) + 2B_Y - C\dot{Y}_1 - KY_1 = m_2\ddot{Y}_1 \\ &\sum M = 0 \Rightarrow C_Y = B_Y \end{aligned} \tag{14}$$

Derivation of Eq. (2) with respect to the yields the following equations:

$$\left.\begin{aligned} &\dot{Y}_1 = \dot{Y}_2 + 2L_1\dot{\theta}\cos\theta \\ &\ddot{Y}_1 = \ddot{Y}_2 + 2L_1\left[\ddot{\theta}\cos\theta - \dot{\theta}^2\sin\theta\right] \end{aligned}\right\} \tag{15}$$

Using Eqs. (14) and (15) yields:

$$\begin{aligned} &m_2\ddot{Y}_2 + \left(2m_2L_1\cos\theta\right)\ddot{\theta} - \left(2m_2L_1\sin\theta\right)\dot{\theta}^2 \\ &= -f_1(t) + 2B_Y - C\dot{Y}_2 - KY_2 \end{aligned} \tag{16}$$

Dynamic force equations of part $\overline{EF}$ are similarly written as follows:

$$\sum F_X = 0 \Rightarrow E_X = F_X$$

$$\sum F_Y = m_2 a_F \Rightarrow -2F_Y = m_2 \ddot{Y}_2 \qquad (17)$$

$$\sum M = 0 \Rightarrow E_Y = F_Y$$

From the matrix form of Eq.(13), B_Y and F_Y are obtained as a function of θ, $\dot{\theta}$, $\ddot{\theta}$, and $\ddot{Y}_2$. Using obtained B_Y and F_Y in Eqs. (16) and (17) yields the following matrix form equations:

$$\begin{bmatrix} \left[-\frac{5m_1L_1}{12\cos\theta} - \frac{m_1L_1(\sin\theta)^2}{4\cos\theta} - \left(2m_2 + \frac{9m_1}{4}\right)(L_1\cos\theta)\right] & (-2m_1 - m_2) \\ \left[-\frac{m_1L_1(\sin\theta)^2}{2\cos\theta} + \frac{3m_1L_1\cos\theta}{2} - \frac{m_1L_1}{6\cos\theta}\right] & \left(m_2 + \frac{3m_1}{2}\right) \end{bmatrix} \begin{bmatrix} \ddot{\theta} \\ \ddot{Y}_2 \end{bmatrix} =$$

$$= \begin{bmatrix} f_1(t) + K\left(Y_2 + 2L_1\sin\theta\right) + C\left(\dot{Y}_2 + 2L_1\dot{\theta}\cos\theta\right) \\ -2L_1\left(m_1 + m_2\right)\dot{\theta}^2\sin\theta \\ 2m_1L_1\dot{\theta}^2\sin\theta \end{bmatrix} \qquad (18)$$

2.4. Dynamic force equations for Maxwell model

Unlike parts $\overline{BC}$ and $\overline{EF}$, dynamic force equations of parts $\overline{AB}$ and $\overline{BF}$ in this model are the same with that of Kelvin–Voigt model. In this model, dynamic force equations of $\overline{EF}$ and $\overline{BC}$ along *y* direction are written as following:

Part $\overline{BC}$: $\sum F_Y = m_2 a_B \Rightarrow -f_1(t) + 2B_Y - C\left(\dot{Y}_1 - \dot{Y}_3\right) = m_2\ddot{Y}_1$

Part $\overline{EF}$: $\sum F_Y = m_2 a_F \Rightarrow -2F_Y = m_2\ddot{Y}_2$ (19)

Viscoelastic components: $F_S = F_C \Rightarrow KY_3 = C\left(\dot{Y}_1 - \dot{Y}_3\right)$

Similar to Kelvin-Voigt model, using Eqs. (13) And (19) give the following matrix form equations:

$$\begin{bmatrix} \left[-\frac{5m_1L_1}{12\cos\theta} - \frac{m_1L_1(\sin\theta)^2}{4\cos\theta} - \left(2m_2 + \frac{9m_1}{4}\right)(L_1\cos\theta)\right] & (-2m_1 - m_2) \\ \left[-\frac{m_1L_1(\sin\theta)^2}{2\cos\theta} + \frac{3m_1L_1\cos\theta}{2} - \frac{m_1L_1}{6\cos\theta}\right] & \left(m_2 + \frac{3m_1}{2}\right) \end{bmatrix} \begin{bmatrix} \ddot{\theta} \\ \ddot{Y}_3 \end{bmatrix} =$$

$$\begin{bmatrix} f_1(t) + K\left(Y_2 + 2L_1\sin\theta\right) + C\left(\dot{Y}_2 + 2L_1\dot{\theta}\cos\theta\right) \\ -2L_1\left(m_1 + m_2\right)\dot{\theta}^2\sin\theta \\ 2m_1L_1\dot{\theta}^2\sin\theta \end{bmatrix} \qquad (20)$$

2.5. General formulation of the models

2.5.1. Kelvin-Voigt model

Using system Eq. (18), $\ddot{\theta}$ and $\ddot{Y}_2$ can be written as functions of t, Y_2, $\dot{Y}_2$, θ, and $\dot{\theta}$ as follows.

$$\left.\begin{aligned}\ddot{\theta} &= F_1\left(t,\theta,\dot{\theta},Y_2,\dot{Y}_2\right)\\ \ddot{Y}_2 &= F_2\left(t,\theta,\dot{\theta},Y_2,\dot{Y}_2\right)\end{aligned}\right\} \tag{21}$$

where the boundary conditions are: $Y_2(0)=0$, $\dot{Y}_2(0)=0$, $\theta(0)=\theta_0$, and $\dot{\theta}(0)=0$

2.5.2. Maxwell model

Similarly, using system Eq.(20), $\ddot{\theta}$ and $\ddot{Y}_3$ can be written as functions of t, Y_3, $\dot{Y}_3$, θ, and $\dot{\theta}$ as shown below:

$$\left.\begin{aligned}\ddot{\theta} &= F_3\left(t,\theta,\dot{\theta},Y_3,\dot{Y}_3\right)\\ \ddot{Y}_3 &= F_4\left(t,\theta,\dot{\theta},Y_3,\dot{Y}_3\right)\end{aligned}\right\} \tag{22}$$

where the boundary conditions are: $Y_3(0)=0$, $\dot{Y}_3(0)=0$, $\theta(0)=\theta_0$, and $\dot{\theta}(0)=0$.

3. Numerical Solution

In here, a numerical solution for solving Eqs (21) and (22) is presented. After solving the equations from this approach, all variables used can be calculated numerically. The numerical solution approach is as follows.

First, the domain of t is divided into n time step, Δt (in here: n=1000). Then, in order to use boundary conditions of the equations, two time step are defined at $t < 0$ as shown in Fig. 7. After that, t(i), $\theta(i)$, and $Y_2(i)$ are defined as $t, \theta(t)$, and $Y_2(t)$ at i^{th} time step. Therefore, the following equation can be used to determine $t(i)$:

$$t(i)=\frac{t_0}{n}(i-3) \tag{23}$$

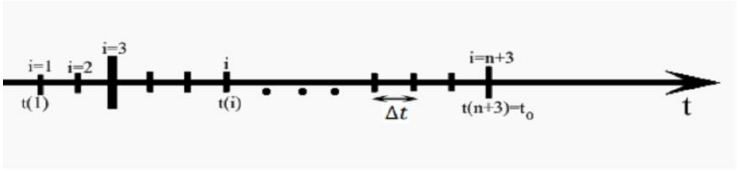

Fig. 7. The time step defined for time domain in numerical solution.

Based on definition of $\dot{\theta}$, $\ddot{\theta}$, $\dot{Y}_2$ and $\ddot{Y}_2$, the following equations were used to solve Eq. (21) numerically:

$$\left.\begin{aligned}
&\dot{\theta}(i)=\frac{\theta(i+1)-\theta(i-1)}{2\Delta t}\\
&\ddot{\theta}(i)=\frac{\dot{\theta}(i+1)-\dot{\theta}(i-1)}{2\Delta t}=\frac{\theta(i+2)-\theta(i-2)}{4(\Delta t)^2}\\
&\dot{Y}_2(i)=\frac{Y_2(i+1)-Y_2(i-1)}{2\Delta t}\\
&\ddot{Y}_2(i)=\frac{\dot{Y}_2(i+1)-\dot{Y}_2(i-1)}{2\Delta t}=\frac{Y_2(i+2)-Y_2(i-2)}{4(\Delta t)^2}
\end{aligned}\right\} \tag{24}$$

where the boundary conditions are: $\theta(1)=\theta(2)=\theta(3)=\theta_0$, $Y_2(1)=Y_2(2)=Y_2(3)=0$ and $\dot{Y}_2(1)=\dot{Y}_2(2)=\dot{Y}_2(3)=0$.

Now, values of θ and Y_2 for Kelvin-Voigt model at different times are determined using the following steps:

Step 1: setting $i=3$ in Eq. (24) yields $\theta(4)$, and $Y_2(4)$ for Kelvin-Voigt model.

Step 2: For $i=3$ to *n*, the following equations are used to determine $\theta(5)$ to $\theta(n+3)$ and $Y_2(5)$ to $Y_2(n+3)$:

$$\left.\begin{aligned}
&\theta(i+2)=4(\Delta t)^2\ddot{\theta}(i)+\theta(i-2)\\
&Y_2(i+2)=4(\Delta t)^2\ddot{Y}_2(i)+Y_2(i-2)
\end{aligned}\right\} \tag{25}$$

Obtaining θ and Y_2 numerically from the mentioned approach, and using Eqs. (2) and (15) and rigid rod body force diagram shown in Fig. 5, $f_2(t)$ can be calculated as follows:

$$\begin{aligned}
&f_2(t)=F=KY_1+C\dot{Y}_1\\
&=K\left[Y_2+2L_1(\sin\theta-\sin\theta_0)\right]+C\left[\dot{Y}_2+2L_1\dot{\theta}\cos\theta\right]
\end{aligned} \tag{26}$$

Similarly, the same numerical solution approach has been performed to solve Eq. (22) for Maxwell model to obtain numerical functions θ and Y_3. Referring to body force diagram for rigid rod, after solving the abovementioned equations, $f_2(t)$ can be calculated numerically using the following equation:

$$f_2(t)=F=KY_3 \tag{27}$$

4. Dynamic Analysis Using Numerical Prediction

In this research, dynamic analysis of viscoelastic star honeycomb structure was carried out by which eight different cases of the model were taken into consideration as shown in Table 1. Using dynamic equation for parts $\overline{AB}$, $\overline{AF}$, $\overline{BC}$ and $\overline{EF}$, two nonlinear coupled differential equations were obtained. Then, a numerical solution was offered to solve the equations during the impact time, [0, t_0]to calculate f_2 and θ as a function of *t*. A linear impact load function and a nonlinear one were used. Graphical representation of results is shown in Fig. 8. The values of *C*, *K*, and t_0 used in this study are 50 N.s/m, 20 kN/m, and 0.05 s, respectively. The primary results are outlined as follows

(i) As the value of initial θ, increases the impact load transmitted to foundation, f_2, is reduced as shown in Figs. 8(a) and 8(b). This is due to more auxeticity of the structure which results in increasing the ability of impact resistance and energy absorption of the structure.

(ii) The value of m_1, increases as the value of f_2 decreases. The reason is that a fraction of impact load f_1 is used to accelerate the structure.

(iii) Two impact load function for $f_1(t)$ was taken into consideration which are $f_1(t)=(20000000)t^3$, and $f_1(t)=(50000)t$. Although the value of $f_1(t_0)$ is the same for both linear and nonlinear load functions, the value of $f_2(t)$ is not the same because of the nonlinearity of the system as shown in Figs. 8(c) and 8(d).

(iv) In this present study, the value of f_2 in Kelvin-Voigt model is less than that in Maxwell model

This present research can be considered as an initial step for designing of viscoelastic auxetic structures with controllable impact resistance and energy absorption ability. The values of design parameters could be chosen in the way that desired transmitted load function would be obtained. It also clarifies that auxetic structure has benefit to be used in a compression type of loading, in addition to tension type of loading normally done by previous researchers. In this research, the technique used for solving nonlinear coupled differential equations can contribute to solve too complicated differential equations without any limitations.

Table. 1. Viscoelastic model and values of parameters in 8 different case.

Model No.	Viscoelastic model	θ (deg)	m_1(kg)	$f_1(t)$ (N)
1	Kelvin-Voigt	30	0.1	$(20000000)t^3$
2	Kelvin-Voigt	60	0.1	$(20000000)t^3$
3	Kelvin-Voigt	30	0.5	$(20000000)t^3$
4	Kelvin-Voigt	30	0.1	$(50000)t$
5	Maxwell	30	0.1	$(20000000)t^3$
6	Maxwell	60	0.1	$(20000000)t^3$
7	Maxwell	30	0.5	$(20000000)t^3$
8	Maxwell	30	0.1	$(50000)t$

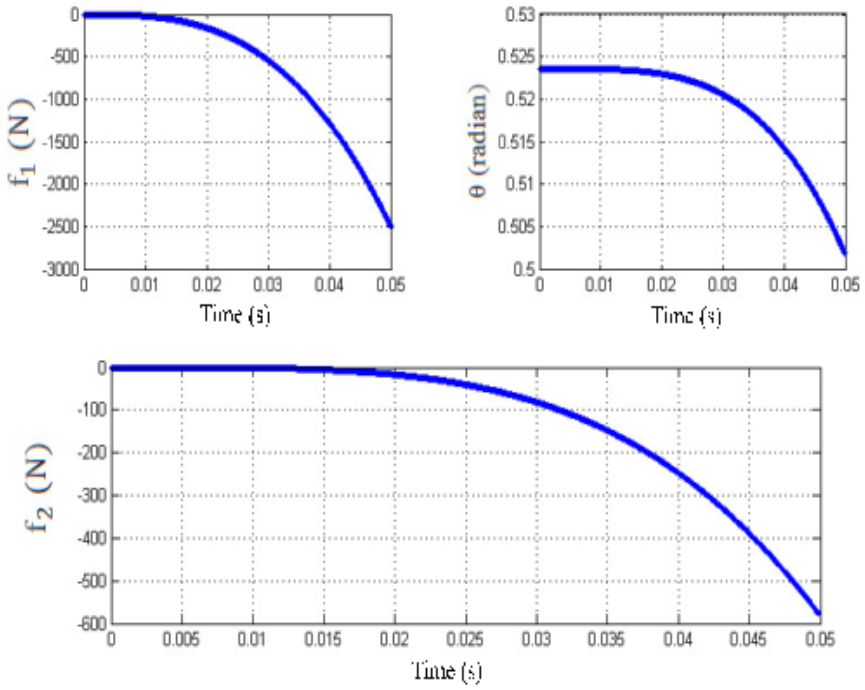

Fig. 8. (a) Case 1

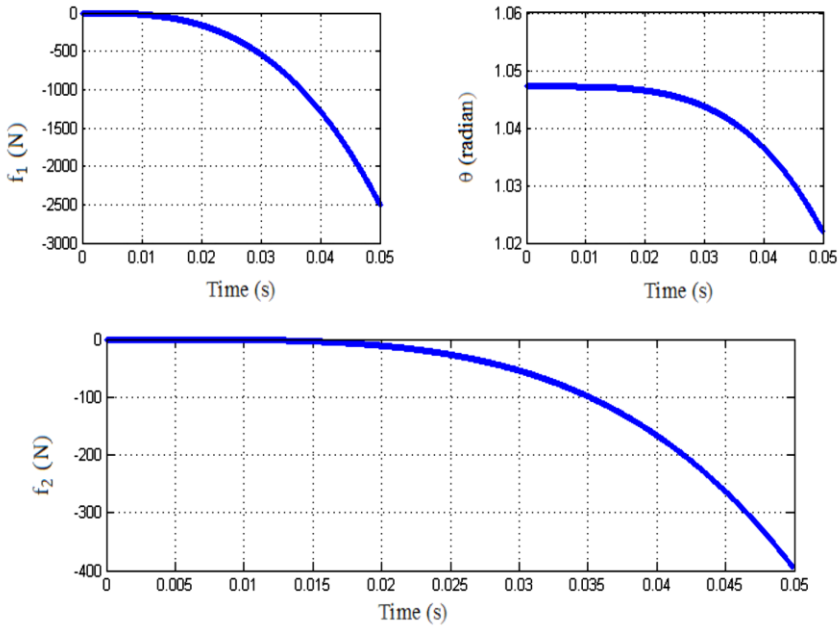

Fig. 8. (b) Case 2

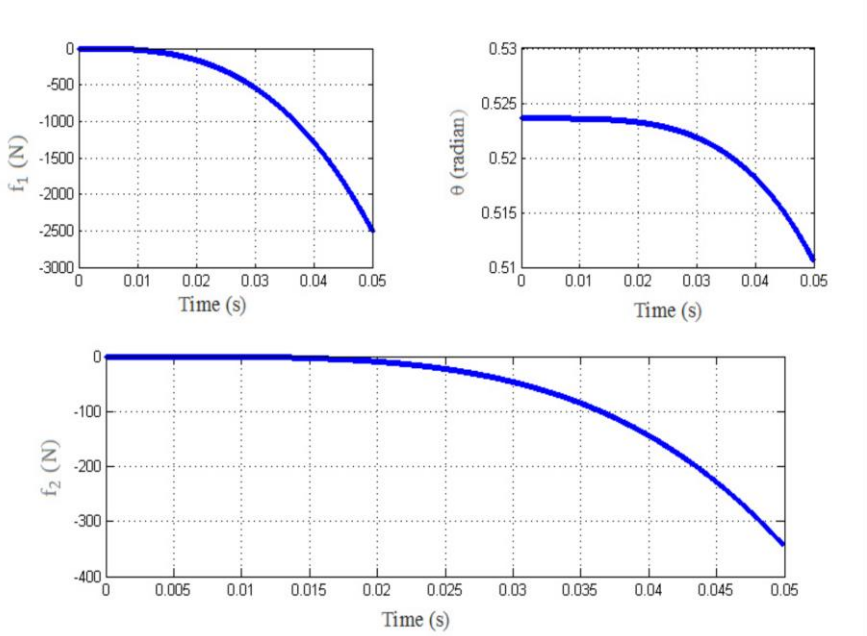

Fig. 8. (c) Case 3

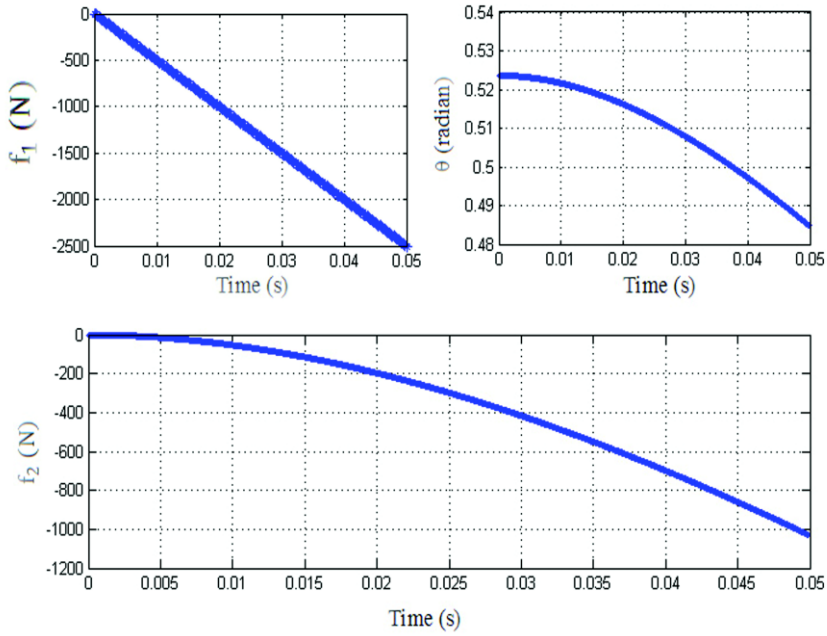

Fig. 8. (d) Case 4

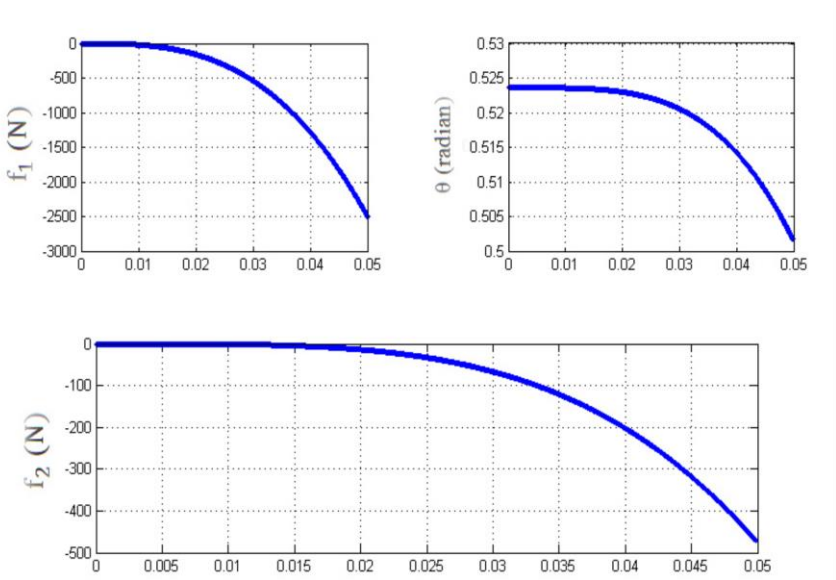

Fig. 8. (e) Case 5

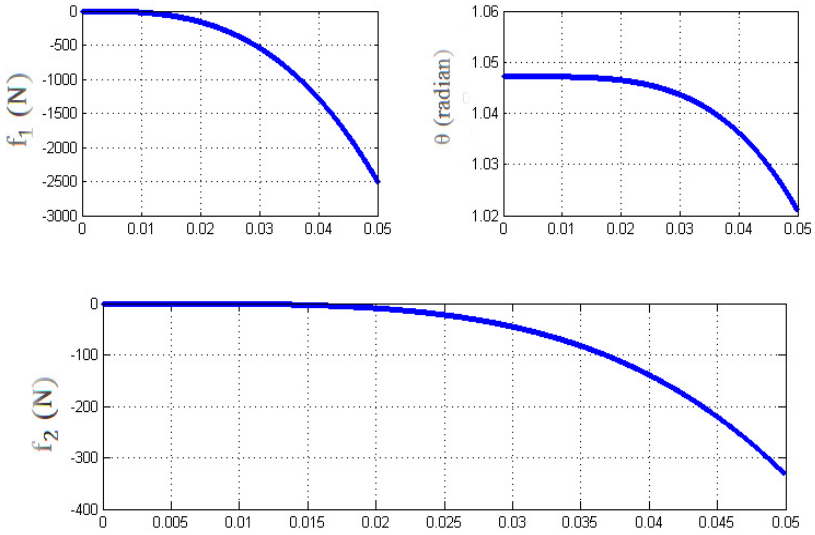

Fig. 8. (f) Case 6

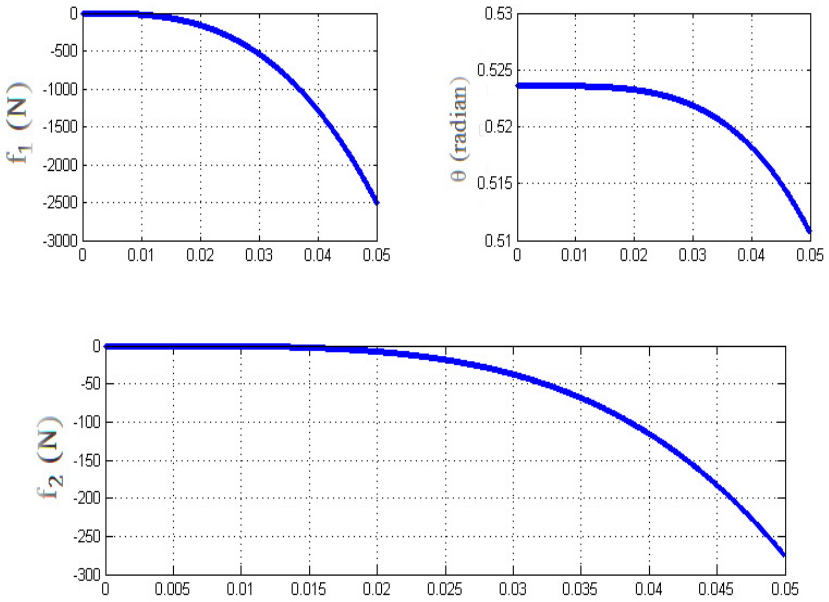

Fig. 8. (g) Case 7

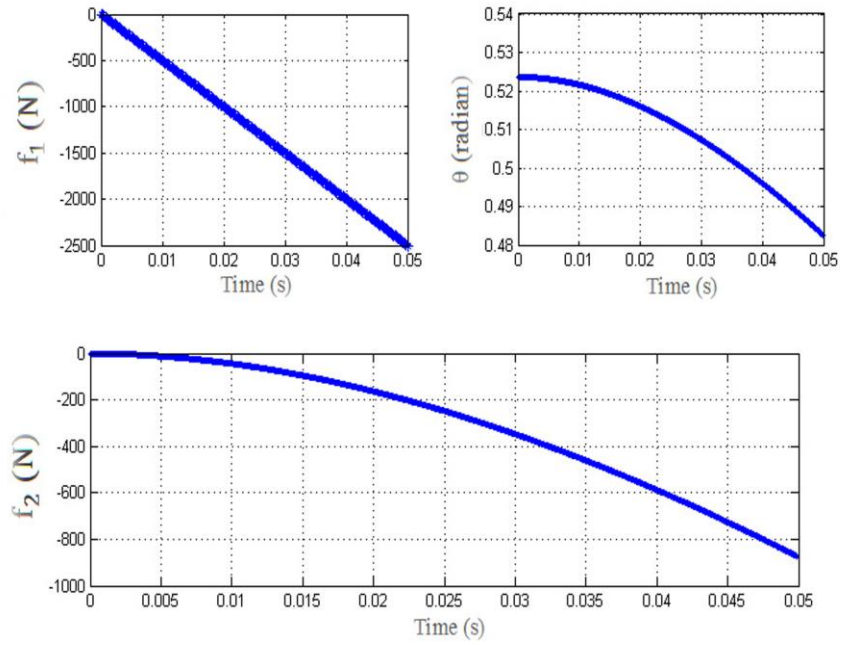

Fig. 8. (h) Case 8

Fig. 8. Functions of $\theta(t)$ and $f_2(t)$ obtained from numerical solution.

5. Conclusion

This paper has developed a design of viscoelastic auxetic honeycomb structures in conjunction with the development of mathematical formulation for structural impact application under dynamic loading. Dynamic analysis has been carried out for the viscoelastic auxetic honeycomb structures leading to the development of empirical formulation to obtain their impact resistance of auxetic structure.

- The proposed viscoelastic component in auxetic structures has merit since the topology allows more degrees of freedom to the auxetic structure such as geometrical parameters of the cell, mass, *K*, *C*, and type of viscoelastic material model.
- The amount of energy absorption capacity of the auxetic material under dynamic loading may numerically been controlled by varying the geometrical and material parameters.
- This pioneer work may be considered as a first attempt in using viscoelastic materials in structural impact application and also provides a basis in designing auxetic structures.

Acknowledgement

Funding by the Ministry of Higher Education (MOHE), Government of Malaysia through Research University Grant UTM: Q.J130000.2624.10J76, Fundamental Research Grant Scheme: R.J130000.7824.4F248 and Flagship Grant: Q.J130000.2424.03G71 is sincerely acknowledged.

References

1. Ahmad, Z.; and Thambiratnam, D.P. (2009). Dynamic computer simulation and energy absorption of foam-filled conical tubes under axial impact loading. *Computers & Structures*, 87(3-4), 186-197.
2. Prawoto, Y. (2012). Seeing auxetic materials from the mechanics point of view: a structural review on the negative Poisson's ratio. *Computational Materials Science*, 58, 140-153.
3. Mohsenizadeh, S.; Alipour, R.; Rad, M.S.; Nejad, A.F.; and Ahmad, Z. (2015). Crashworthiness assessment of auxetic foam-filled tube under quasi-static axial loading. *Materials & Design*, 88, 258-268.
4. Mohsenizadeh, S.; Alipour, R.; Ahmad, Z.; and Alias, A. (2016). Influence of auxetic foam in quasi-static axial crushing. *International Journal of Materials Research*, 107(10), 916-924.
5. Rad, M.S.; Prawoto, Y.; and Ahmad, Z. (2014). Analytical solution and finite element approach to the 3D re-entrant structures of auxetic materials. *Mechanics of Materials*, 74, 76-87.
6. Liu, Y.; and Hu, H. (2010). A review on auxetic structures and polymeric materials. *Scientific Research and Essays*, 5(10), 1052-1063
7. Theocaris, P.S.; and Stavroulakis, G.E. (1998). The homogenization method for the study of variation of Poisson's ratio in fiber composites. *Archive of Applied Mechanics*, 68(3-4), 281-295.

8. Lim, T.C. (2003). Constitutive relationship of a material with unconventional Poisson's ratio. *Journal of Materials Science Letters*, 22(24), 1783-1786.
9. Grima, J.N.; Gatt, R.; Alderson, A.; and Evans, K.E. (2005). On the potential of connected stars as auxetic systems. *Molecular Simulation*, 31(13), 925-935.
10. Spadoni, A.; Ruzzene, M.; and Scarpa, F. (2005). Global and local linear buckling behavior of a chiral cellular structure. *Physica Status Solidi (b)*, 242(3), 695-709.
11. Bornengo, D.; Scarpa, F.; and Remillat, C. (2005). Evaluation of hexagonal chiral structure for morphing airfoil concept. *Proceedings of the Institution of Mechanical Engineers, Part G: Journal of Aerospace Engineering*, 219(3), 185-192.
12. Li, Y. (1976). The anisotropic behavior of Poisson's ratio, Young's modulus, and shear modulus in hexagonal materials. *Physica Status Solidi (a)*, 38(1), 171-175.
13. Grima, J.N.; Gatt, R.; Ravirala, N.; Alderson, A.; and Evans, K.E. (2006). Negative Poisson's ratios in cellular foam materials. *Materials Science and Engineering: A*, 423(1), 214-218.
14. Grima, J.N.; Gatt, R.; Alderson, A.; and Evans, K.E. (2005). On the auxetic properties of rotating rectangles' with different connectivity. *Journal of the Physical Society of Japan*, 74(10), 2866-2867.
15. Milton, G.W. (1992). Composite materials with Poisson's ratios close to -1. *Journal of the Mechanics and Physics of Solids*, 40(5), 1105-1137.
16. Hine, P.J.; Duckett, R.A.; and Ward, I.M. (1997). Negative Poisson's ratios in angle-ply laminates. *Journal of Materials Science Letters*, 16(7), 541-544.
17. Wojciechowski, K.W. (2003). Remarks on Poisson ratio beyond the limits of the elasticity theory. *Journal of the Physical Society of Japan*, 72(7), 1819-1820.
18. Wojciechowski, K.W. (2003). Non-chiral, molecular model of negative Poisson ratio in two dimensions. *Journal of Physics A: Mathematical and General*, 36(47), 11765.
19. Tretiakov, K.V.; and Wojciechowski, K.W. (2007). Poisson's ratio of simple planar 'isotropic'solids in two dimensions. *Physica Status Solidi (b)*, 244(3), 1038-1046.
20. Alderson, A.; and Alderson, K.L. (2007). Auxetic materials. *Proceedings of the Institution of Mechanical Engineers, Part G: Journal of Aerospace Engineering*, 221(4), 565-575.
21. Alderson, K.L.; Alderson, A.; and Evans, K.E. (1997). The interpretation of the strain-dependent Poisson's ratio in auxetic polyethylene. *The Journal of Strain Analysis for Engineering Design*, 32(3), 201-212.
22. He, C.; Liu, P.; McMullan, P.J.; and Griffin, A.C. (2005). Toward molecular auxetics: Main chain liquid crystalline polymers consisting of laterally attached para-quaterphenyls. *Physica Status Solidi (b)*, 242(3), 576-584.
23. Aldred, P.; and Moratti, S.C. (2005). Dynamic simulations of potentially auxetic liquid-crystalline polymers incorporating swivelling mesogens. *Molecular Simulation*, 31(13), 883-887.

24. Ren, X.; Shen, J.; Ghaedizadeh, A.; Tian, H.; and Xie, Y.M. (2016). A simple auxetic tubular structure with tuneable mechanical properties. *Smart Materials and Structures*, 25(6), 065012.
25. Mukhopadhyay, T.; and Adhikari, S. (2016). Effective in-plane elastic properties of auxetic honeycombs with spatial irregularity. *Mechanics of Materials*, 95, 204-222.
26. Rad, M.S.; Ahmad, Z.; and Alias, A. (2015). Computational approach in formulating mechanical characteristics of 3D star honeycomb auxetic structure. *Advances in Materials Science and Engineering*, Volume 2015, Article ID 650769, 11 pages.